Chapter 1

Novel Theoretical Approaches for Understanding and Predicting Dislocation Evolution and Propagation

Binh Duong Nguyen, Stefan Sandfeld

1.1 Introduction

Dislocations in semiconductors have been studied extensively for Si and GaAs, both of which have a face centred cubic crystal structure. Such crystal boules are grown from the melt using the Czochralski and floating zone method in the case of Si, and liquid encapsulated Czochralski and vertical gradient freeze method in the case of GaAs. The application of the so-called Dash necking technique [1] allows the reduction of the dislocation density in Si during the initial seeding growth stage down to a zero dislocation density value and then to retain this state throughout the complete growth process. Si ingots of up to 450 mm in diameter and wafers cut from those with a dislocation density of $0\,\mathrm{cm}^{-2}$ nowadays can be considered state of the art. GaAs as compared to Si has different thermo-elastic properties and exhibits a greater brittleness, which is why growth of "zero dislocation" GaAs succeeded only up to a crystal diameter of roughly 70 mm [2]. GaAs crystal boules with a diameter >100 mm exhibit dislocation densities of approximately $100\,\mathrm{cm}^{-2}$ to $3000\,\mathrm{cm}^{-2}$. There, dislocations often cluster or form dislocation networks, sometimes termed *dislocation patterns*, that consist in a inhomogeneous dislocation distribution with regions of very low density bounded by strongly localized regions of very high densities. Due to the performance killing impact of dislocations on electronic devices, their propagation, multiplication and annihilation has been studied in many aspects. Usually, the study of dislocation behavior during bulk growth is related to thermo-elastic strain in the growing crystal. For a recent overview please refer to the "Handbook of crystal growth – bulk growth" edited by P. Rudolph [3] and to the recent work [4, 5] which particularly considers the formation of cellular dislocation networks also in SiC. Besides high dislocation densities and small angle grain boundaries,

also micro-pipes and super-screw dislocations with Burgers vectors larger than the c-lattice parameter are an important issue in SiC growth [6]. Last but not least stacking faults together with the occurring partial dislocations of different core structures form extended defects, especially in non-cubic semiconductors such as nitrides and SiC [6]. This makes SiC a particularly interesting model system for defects in non-cubic semiconductor crystals.

In the following, we first introduce the state of the art in terms of modeling and simulation approaches. After that we concentrate on continuum modeling approaches for dislocation emphasis on two specific model classes, the Alexander-Haasen model and continuum dislocation dynamics models. This is followed by numerical examples that demonstrate different features of evolving dislocation structures: the first example shows that the ability to represent the flow of dislocations is important; the second example deals with dislocation motion between dislocation veins which act as strong obstacles for the motion of dislocations. We then summarize our work and put it into the perspective of ongoing research.

1.2 General Modeling and Simulation approaches

There are many modeling and simulation approaches for defect-related phenomena on (sub) nanometer length scales. E.g., in the context of defects in semiconductors, Łażewski [7] used density function theory for investigating the electrostatic barrier near the core of a pair of edge dislocations, and a number of authors, among them Rao [8], Oren [9], Zhou [10], Chen [11] applied molecular dynamics simulation for simulating dislocation in various materials such as, e.g., B3-GaN. However, such simulations are – for reasons of computational cost – not appropriate for simulating the structure-property relation of specimens on a macroscopic length scale. Discrete dislocation dynamics (DDD) simulations [12–17] have been used only in rare cases with simulation codes from the metal plasticity community [18] and also suffer from a large computational cost. Nonetheless, they are able to simulate larger volumes/numbers of interacting dislocations than atomistic simulations. In the field of metal plasticity, phase field methods for dislocation dynamics gained some popularity [19, 20]. They do not resolve individual atoms but are still able to represent the dislocation core energy in some physical detail – unlike the DDD methods most of which are based on linear elasticity approaches. So far, there have been no applications to the domain of semiconductors.

Most of the (commercially) available software for macroscopic modeling on the device scale of semiconductors usually is only able to computes thermal stress during the growth process and, based on this, to roughly estimates the dislocation density based on a resolved shear stress; neither strain hardening nor details of the nucleation process or the flow of dislocations can be considered. Among the most commonly used phenomenological model is the Alexander-Haasen model (AH model) [21], which is utilized in a range of different formulations to semi-quantitatively describe dislocation structures. [22, 23] developed an elastic-viscoplastic type of constitutive equation for predicting the quantity of dislocation density. Ide [24] analyzed the influence of oxygen diffusion on dislocation density during crystal growth and during the cooling processes. State of the art simulation methods furthermore embed the AH model into a crystal plasticity finite element model [25–27] and thereby also consider the influence of the crystallographic orientations and slip systems on the resolved shear stress.

A novel type of continuum models is motivated by work that, so far, has been undertaken only within the small-scale metal plasticity field. The so-called Continuum Dislocation Dynamics (CDD) theory [28–32] is a strongly enhanced continuum crystal plasticity formulations in terms of additional microstructural information (i.e. detailed geometrical information of dislocation) and their non-local evolution equations (describing dislocation flow). The result is a continuum theory that is almost as detailed as a discrete dislocation dynamics model but that does not suffer from the same computational restriction [33]: the computational time in DDD simulations scales almost quadratically with the number of interacting line segments, while for the CDD theory the number of dislocations has no influence, which allows for computational models that can eventually reach length and time scales comparable to experimental ones. As opposed to other continuum approaches, CDD can naturally differentiate and convert between straight and curved dislocations, as well as between 'geometrically necessary dislocations' (GNDs) and 'statistically stored dislocations' (SSDs) [31, 29].

1.3 Continuum Dislocation Modelling approaches

Continuum models for predicting the evolution of dislocations have been used for more than half a century. The popularity is a result of the fact that continuous representations do not resolve each individual dislocation but rather operate with continuous density fields. The benefit is that the computational cost can be strongly reduced due to the fact that a density, i.e., the *dislocation line length per volume* is just a single number regardless how many dislocations are present. Thus, the computational cost does not scale with the number of interacting dislocations or atoms. The drawback is that a density value is not able to represent all details of the potentially complex dislocation microstructure [34–36]. In the following, we will introduce the theoretical background of two different models, the Alexander-Haasen model and the Continuum Dislocation Dynamics theory.

1.3.1 Alexander-Haasen model

The Alexander-Haasen (AH) model [21] is based on the standard assumption of additive decomposition of the total strain rate $\dot{\boldsymbol{\varepsilon}}$ into an elastic part $\dot{\boldsymbol{\varepsilon}}^{\mathrm{el}}$, a thermal part $\dot{\boldsymbol{\varepsilon}}^{\mathrm{th}}$ and a plastic contribution $\dot{\boldsymbol{\varepsilon}}^{\mathrm{pl}}$ as, $\dot{\boldsymbol{\varepsilon}} = \dot{\boldsymbol{\varepsilon}}^{\mathrm{el}} + \dot{\boldsymbol{\varepsilon}}^{\mathrm{th}} + \dot{\boldsymbol{\varepsilon}}^{\mathrm{pl}}$. Thermal loading causes thermal eigenstrains $\boldsymbol{\varepsilon}^{\mathrm{th}}$, while the mechanical loading gives rise to elastic strains $\boldsymbol{\varepsilon}^{\mathrm{el}}$, and additionally the presence of dislocations causes eigenstrains $\boldsymbol{\varepsilon}^{\mathrm{pl}}$. Explicitly solving the (anisotropic) elastic boundary value problem yields stresses $\boldsymbol{\sigma}$. Projecting those by application of the symmetric projection tensor $\boldsymbol{M}_s = \boldsymbol{n} \otimes \boldsymbol{s}$, with the slip plane normal vector $\boldsymbol{n}$ and the slip direction $\boldsymbol{s}$ gives resolved shear stresses τ_{res} in the local coordinate system of the respective slip systems s. The plastic shear strain contribution to $\boldsymbol{\varepsilon}^{\mathrm{pl}}$ in the slip coordinate system is obtained from the Orowan equation, $\dot{\epsilon}^{\mathrm{pl}} = \rho_{\mathrm{m}} b v$, with the modulus of the Burgers vector b, the density of mobile dislocations ρ_{m} and the velocity of mobile dislocations v. The latter is phenomenologically given as a function of temperature and local effective stress

$$v = v_0 \left(\frac{\tau_{\mathrm{eff}}}{\tau_0} \right)^m \exp\left(-\frac{Q}{k_{\mathrm{B}} T} \right) \mathrm{sign}(\tau_{\mathrm{res}}) \tag{1.1}$$

where k_B is the Boltzmann constant, Q is the activation enthalpy, T is the temperature, and m is a fitting parameter. Furthermore, the effective shear stress is

$$\tau_\mathrm{eff} = \langle |\tau_\mathrm{res}| - \tau_\mathrm{y} \rangle \qquad \text{with} \quad \langle \cdot \rangle = \begin{cases} \langle \cdot \rangle \text{ for } \langle \cdot \rangle > 0 \\ 0 \text{ for } \langle \cdot \rangle \leq 0 \end{cases} . \tag{1.2}$$

Therein, the yield stress τ_y governs dislocation interactions and is given by the so-called Taylor relation [37], $\tau_\mathrm{y} = aGb\sqrt{\rho_\mathrm{m}}$, with a constant a typically in the range of $0.2 \ldots 0.5$ and the shear modulus G. The yield stress acts like a friction stress which has to be overcome for plastic activity to take place. The set of equations is completed by a constitutive rate expression for the dislocation density of the form

$$\dot{\rho}_\mathrm{m} = K \left(\frac{\tau_\mathrm{eff}}{\tau_0} \right)^\lambda \rho_\mathrm{m} |v|, \tag{1.3}$$

with parameters λ and τ_0. Model extensions may separately consider evolution equations for mobile and immobile dislocations but are not able to convert the former into the latter quantity, or vice versa (cf. [38] for a discussion of the shortcomings of these models).

This macroscopic constitutive model might be used for obtaining a rough estimate of the order of magnitude of dislocation density in situations where homogeneous plasticity can be assumed. However, it is generally not possible to decide a priori whether homogeneous plasticity can be assumed or not. The AH-model fails to predict fluxes of dislocations since it is a local model, given as an ordinary differential equation. It therefore also cannot represent, e.g., loss of dislocations through surfaces, as has been investigated in more details in [39]. Another consequence is that it fails to predict the peculiarities of occurring heterogeneous dislocation microstructures as e.g. during dislocation cell structure formation. Thus, the AH model has only a limited range of applicability.

1.3.2 Continuum Dislocation Dynamics models

Any version of a Continuum Dislocation Dynamics model is a non-local model which was obtained by coarse-graining the geometrical properties and the motion of discrete dislocations (the so-called *kinematics* of dislocations). As such, it is based on a set of continuous variables and describes at least the *flux* of dislocation density by a set of transport equations. These models have been developed for and so far mainly used in the domain of metal plasticity [40–43, 31, 29].

The simplest model: straight parallel dislocation with the same line direction

In the particular case of straight dislocations of the same line direction, running along the y direction of a Cartesian coordinate system and that move in a slip system with $\boldsymbol{n} = \boldsymbol{e}_\mathrm{z}$, the continuum dislocation kinematics is described by a scalar evolution equation of dislocation density ρ

$$\partial_\mathrm{t} \rho = -\partial_\mathrm{x} \left(\rho v \right), \tag{1.4}$$

where $\partial_i(\cdot) \equiv \partial(\cdot)/\partial i$. For a constant dislocation velocity v this would be a pure convection equation. It is accompanied by the Orowan equation

$$\partial_\mathrm{t}\gamma = \rho v b, \tag{1.5}$$

where b is the magnitude of the Burgers vector and γ is the plastic shear strain in the respective slip system. γ, as an eigenstrain, serves as the connection to the elasticity theory, similar as in the AH model. The resulting stresses reflect in the velocity function v as detailed below.

The "Groma" model: straight parallel dislocations with two line directions

Among those who established a more general continuum model in the dislocation community were van der Giessen and Needleman [44] as well as I. Groma [45, 28] who additionally investigated how the interaction of dislocations can be described in terms of continuum variables. The evolution equation Eq. 1.4 is then replaced by a set of evolution equations for the total and signed GND densities as,

$$\begin{aligned} \partial_\mathrm{t}\rho_\mathrm{tot} &= -\partial_x(\rho_\mathrm{gnd}\, v) \\ \partial_\mathrm{t}\rho_\mathrm{gnd} &= -\partial_x(\rho_\mathrm{tot}\, v). \end{aligned} \tag{1.6}$$

Dislocation densities still describe only straight (edge) dislocation, but this model allows for two different line orientations. The positive and negative dislocation densities, ρ_+ and ρ_-, are then defined as the number of dislocations with positive or negative line direction per averaging area. Thus, the total and GND density can be alternatively expressed as

$$\rho_\mathrm{tot} = \rho_+ + \rho_- \tag{1.7}$$

$$\rho_\mathrm{gnd} = \rho_+ - \rho_-. \tag{1.8}$$

Fig. 1.1 shows a sketch of two different dislocation configurations highlighting the need for *two* different density variables. In the Groma model, it is possible to represent a so-called statistically stored dislocation (SSD) content inside an averaging volume, e.g., the volume contains both an edge dislocation with positive line orientation and an edge dislocation with negative line orientation. As a consequence, positive and negative densities can move past each other without being annihilated, i.e., as if on different slip planes inside the averaging volume.

The Kröner-Nye model for geometrically necessary dislocations

A different approach is based on the Kröner-Nye tensor [46] which is defined as

$$\boldsymbol{\alpha} = \operatorname{curl} \boldsymbol{\beta}_\mathrm{pl}, \tag{1.9}$$

where $\boldsymbol{\beta}_\mathrm{pl}$ is the plastic distortion. This representation is only valid if all dislocations in an averaging volume share the same line direction $\boldsymbol{l}$, which is why there is an alternative formulation based on the GND density,

$$\boldsymbol{\alpha} = \rho_\mathrm{gnd} \boldsymbol{l} \otimes \boldsymbol{b}. \tag{1.10}$$

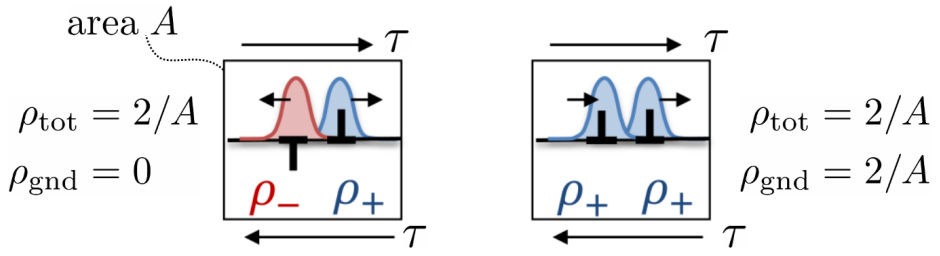

Figure 1.1: Left: an averaging area containing two edge dislocations with opposite line directions. Right: same averaging area containing two edge dislocations with the same line direction. Both systems have the same total density but differ in the net GND content. τ is the applied shear stress under which action a positive edge dislocations moves in positive x direction (here: to the right), a negative edge moves towards the left, as indicated by the small arrows.

If the coordinate system is aligned with the Burgers vector direction and the edge orientation, the individual coefficients of the Kröner-Nye tensor contain the edge and screw GND contributions. One of the main differences to the above introduced two models is that here dislocations can also be curved. A serious drawback of this quantity is that once the assumption of GND content is violated, e.g., an averaging volume contains dislocations of opposite line orientation, the dislocation content would be "annihilated". This is nonphysical in particular in situations where averaging volumes are larger than the annihilation distance which for metals has a typical order of magnitude of a few Burgers vectors. Combining the advantage of the Groma model to handle SSD densities with opposite line orientations with the ability of the Kröner-Nye model to handle arbitrarily curved lines leads to extended Continuum Dislocation Dynamics models that can also work in truly three-dimensional situations.

Three-dimensional Continuum Dislocation Dynamics (CDD)

Representing dislocation microstructures as only straight edge dislocations in 2D or as GND structures has many limitations and is therefore not suitable to be used as basis for 3D models:

(i) Curved dislocations may bow out and thereby increase the line length contained in the system, while straight dislocations can only translate [40]. However, the resulting densities and the plastic slip is very different.

(ii) While only GNDs give rise to internal stresses [45, 32], *all* dislocations need to be considered because due to the motion of dislocations they can change their "character", e.g., a GND configuration may become a dipole configuration with a zero net GND content.

(iii) Real dislocation microstructures are intrinsically three-dimensional and may include many complex phenomena such as junctions or locks that can only be represented in truly three-dimensional models. A detailed comparison of CDD models of varying complexity can be found in [38].

To alleviate the above shortcomings, a more advanced continuum dislocation dynamics model was introduced by Hochrainer, Sandfeld, Zaiser, and Gumbsch [29], which also can be generalized to three-dimensional systems. Similar to the above models, the dislocation velocity drives the evolution of the dislocation microstructure in each slip system, which in the case of Hochrainer's CDD is represented by four field variables: the total density ρ_t (which upon volume integration gives the total line length inside the volume), a vector of "geometrically necessary" dislocation density $\boldsymbol{\varrho} = [\varrho_\mathrm{s}, \varrho_\mathrm{e}]$, e.g. of screw ($\varrho_\mathrm{s}$) and edge ($\varrho_\mathrm{e}$) dislocations, a curvature density q_t (which upon volume integration gives the number of closed dislocation loops as multiple of 2π) and the plastic strain γ. The temporal change is governed by evolution equations (PDEs) which have the character of transport equations

$$\begin{aligned}
\partial_\mathrm{t}\rho_\mathrm{t} &= -\nabla\cdot(v\boldsymbol{\varrho}^\perp) + vq_\mathrm{t}\\
\partial_\mathrm{t}\boldsymbol{\varrho} &= -\nabla(v\rho_\mathrm{t})\\
\partial_\mathrm{t}q_\mathrm{t} &= -\nabla\cdot(-v\boldsymbol{Q}^{(1)} + \boldsymbol{A}^{(2)}\cdot\nabla v)
\end{aligned} \tag{1.11}$$

and which are, for each slip system, completed by the Orowan equation for the rate of plastic strain $\gamma = \rho_\mathrm{t} b v$. Therein, a dot denotes the scalar product, $\boldsymbol{\varrho}^\perp = [\varrho_\mathrm{e}, -\varrho_\mathrm{s}]$ is the 90^0 rotated GND density vector. As stated in [36], we assume that,

$$\boldsymbol{Q}^{(1)} = -\boldsymbol{\varrho}^\perp q_\mathrm{t}/\rho_\mathrm{t} \tag{1.12}$$

$$\boldsymbol{A}^{(2)} = \frac{\rho_\mathrm{t}}{2}\left[(1+\Psi)\,\boldsymbol{l}_\varrho\otimes\boldsymbol{l}_\varrho + (1-\Psi)\,\boldsymbol{l}_{\varrho^\perp}\otimes\boldsymbol{l}_{\varrho^\perp}\right] \tag{1.13}$$

where $\boldsymbol{l}_{\varrho^\perp}$ is the unit vector perpendicular to $\boldsymbol{l}_\varrho$ and $\boldsymbol{l}_\varrho = \boldsymbol{\varrho}/|\boldsymbol{\varrho}|$ is the average line direction, and Ψ is approximated as

$$\Psi \approx \frac{(|\boldsymbol{\varrho}|/\rho_\mathrm{t})^2\left(1+(|\boldsymbol{\varrho}|/\rho_\mathrm{t})^4\right)}{2}. \tag{1.14}$$

Hochrainer et al. [29] showed that it is possible to construct CDD formulations that additionally include higher order equations, which was analyzed for a number of formulations by Monavari et al. [38]. However, Sandfeld and Po [47] showed, that already the above set of equations is well able to represent many important features of DDD simulations.

The velocity v in the above equations needs to be specified in terms of a constitutive equation through which elastic interactions enter the model,

$$v = \begin{cases} \frac{b}{B}\left(|\tau_0| - \tau_\mathrm{y}\right) & \text{for } |\tau_0| > \tau_\mathrm{y} \\ 0 & \text{otherwise} \end{cases}, \tag{1.15}$$

where $\tau_0 = \tau_\mathrm{ext} + \tau_\mathrm{int}$ is the summation of the external shear stress (τ_ext) and the long-range (or 'internal') interaction stresses (τ_int) which have to be obtained from the additional solution of a dislocation eigenstrain problem [48, 49, 32]. τ_y is as above the Taylor type yield stress.

1.4 Example 1: Comparison of the Alexander-Haasen and the Groma model

1.4.1 Governing equations

In the following we only want to study the difference due to the transport character of the evolution equations. To make the two models comparable, we will use the same phenomenological source term for dislocation multiplication of the AH model for the Groma model. By adding the right hand side of Eq.1.3 into the tranport equations (Eq.1.6) with the assumption that $\rho_{\mathrm{tot}} \equiv \rho_{\mathrm{m}}$, the evolution equations (Eq.1.6) then simply become

$$\begin{aligned} \partial_{\mathrm{t}}\rho_{\mathrm{tot}} &= -\partial_x(\rho_{\mathrm{gnd}}v) + S \\ \partial_{\mathrm{t}}\rho_{\mathrm{gnd}} &= -\partial_x(\rho_{\mathrm{tot}}v) \end{aligned} \tag{1.16}$$

with

$$S = K\left(\frac{\tau_{\mathrm{eff}}}{\tau_0}\right)^{\lambda}\rho_{\mathrm{tot}}|v|, \tag{1.17}$$

where v is again given by Eq. 1.1. The subscript "m" in the AH model indicates that only mobile and no sessile dislocations are considered; the Groma model does not have to differentiated between the two "types" of dislocations. However, since in our model no, e.g. junction formation can take place, all dislocations could be considered as mobile.

1.4.2 Physical system and model setup

The considered physical system is a hexagonal 4H-SiC crystal as, e.g., grown by the physical vapor transport (PVT) technique. The crystal is assumed to have h =45 mm and the radius r =30 mm, as shown by the gray shaded region in Fig. 1.2a. As a simplification we only consider a two-dimensional cross-section as indicated by the blue rectangle in the same figure. There, the basal plane which is characterized by a normal pointing into the z direction is the only active slip system. As mechanical boundary conditions the crystal is fixed in the x and z directions at point C_1 and only in z direction at point C_2. For simplicity we do not consider cooling, heating, or heat fluxes, only a time independent symmetrical temperature field is prescribed during simulation. The resulting resolved shear stress distribution is shown in Fig. 1.2. The same geometry setup is used for the AH model and the Groma model. The simulations are based on the following material parameters and constants: $b = 3.073 \times 10^{-10}\,\mathrm{m}$, $v_0 = 8.5 \times 10^{-15}\,\mathrm{m\,s^{-1}}$, $K = 2.0 \times 10^{-5}\,\mathrm{m^{-1}}$, $Q = 3.3\,\mathrm{eV}$, $\lambda = 1.1$, $m = 2.8$, $a = 0.425$, and the Boltzmann constants is $k_{\mathrm{B}} = 8.617 \times 10^{-5}\,\mathrm{eV\,K^{-1}}$. For the mechanical problem the thermal expansion coefficient is temperature dependent [50] as shown in Fig. 1.3; also the components of the stiffness tensor are temperature dependent [51]. In Voigt notation they read for hexagonal SiC: The temperature dependent shear modulus is taken as the elastic

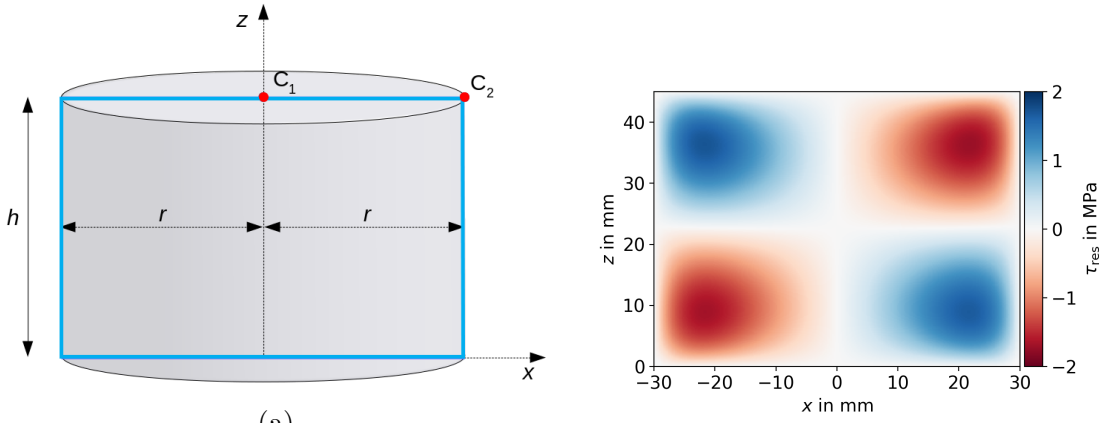

Figure 1.2: (a) 2D crystal geometry and (b) initial distribution of the resolved shear stress τ_{res} at $t = 0$s in the plane indicated by the blue lines in (a).

constant C_{44}.

$$\begin{bmatrix} C_{11} \\ C_{12} \\ C_{13} \\ C_{33} \\ C_{44} \end{bmatrix} = T \times \begin{bmatrix} -0.025 \\ -0.011 \\ -0.011 \\ -0.025 \\ -0.007 \end{bmatrix} \frac{\text{GPa}}{\text{K}} + \begin{bmatrix} 486.6 \\ 101.3 \\ 59.02 \\ 528.9 \\ 150.3 \end{bmatrix} \text{GPa}. \tag{1.18}$$

For the numerical solution of this time dependent, multiphysics problem which consists of a mechanical part, a thermal part and the dislocations part, the finite element method is used. For the numerical discretization, triangular elements with quadratic shape functions were used for both the elastic and thermal problem; for the CDD dislocation problem we used cubic shape functions so that all derivatives are approximated properly.

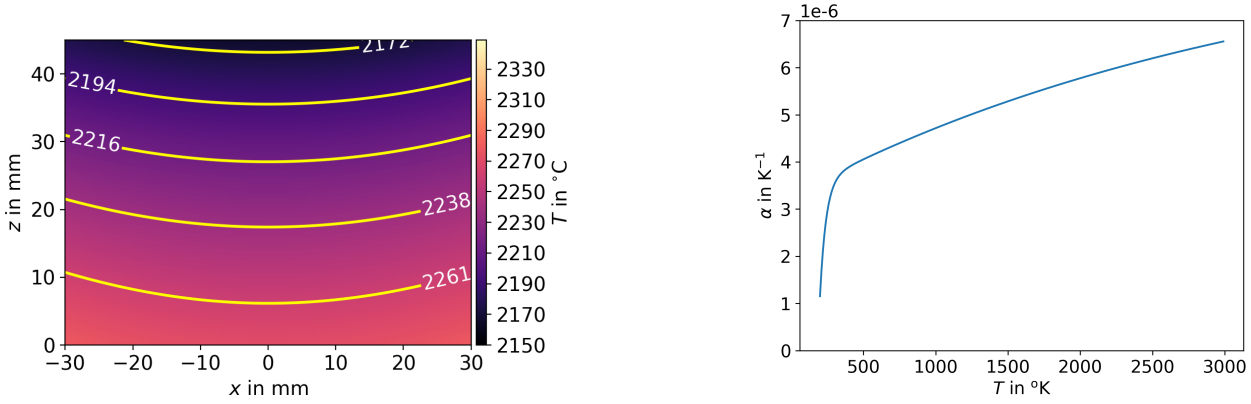

Figure 1.3: Left: thermal expansion coefficient, right: prescribed temperature field

1.4.3 Results and discussion

The simulation results of the AH model and the Groma model are shown in Fig. 1.4 and include dislocation density, resolved shear stress and plastic shear strain at a total time of $t = 3000$s. There, the plots in the left column display the result from the AH model, the middle column shows the results from the Groma model and the last column are the corresponding results along the red, dashed line. The difference between these two model is then easily observable with both the magnitude of dislocation density (Fig. 1.4a and Fig. 1.4b) and the qualitative shape of the plots themselves (see Fig. 1.4c). The AH model shows a growing patch of increasing dislocation density (see Fig. 1.4a) where the resolved shear stress is highest while the Groma model exhibits smaller patches of dislocation density (see Fig. 1.4b) at the surface ($x \approx 30\,\mathrm{mm}$, label C) and around the crystal axis ($x = 0\,\mathrm{mm}$, label A). The maximum dislocation density values of the Groma model are observed to be close to the surface with values of roughly $2500\,\mathrm{cm}^{-2}$ and a value of $600\,\mathrm{cm}^{-2}$ around the axis, while the AH model has a maximum value of approximately $1500\,\mathrm{cm}^{-2}$. In a way, the two models behave opposite to each other. The difference between the two models is

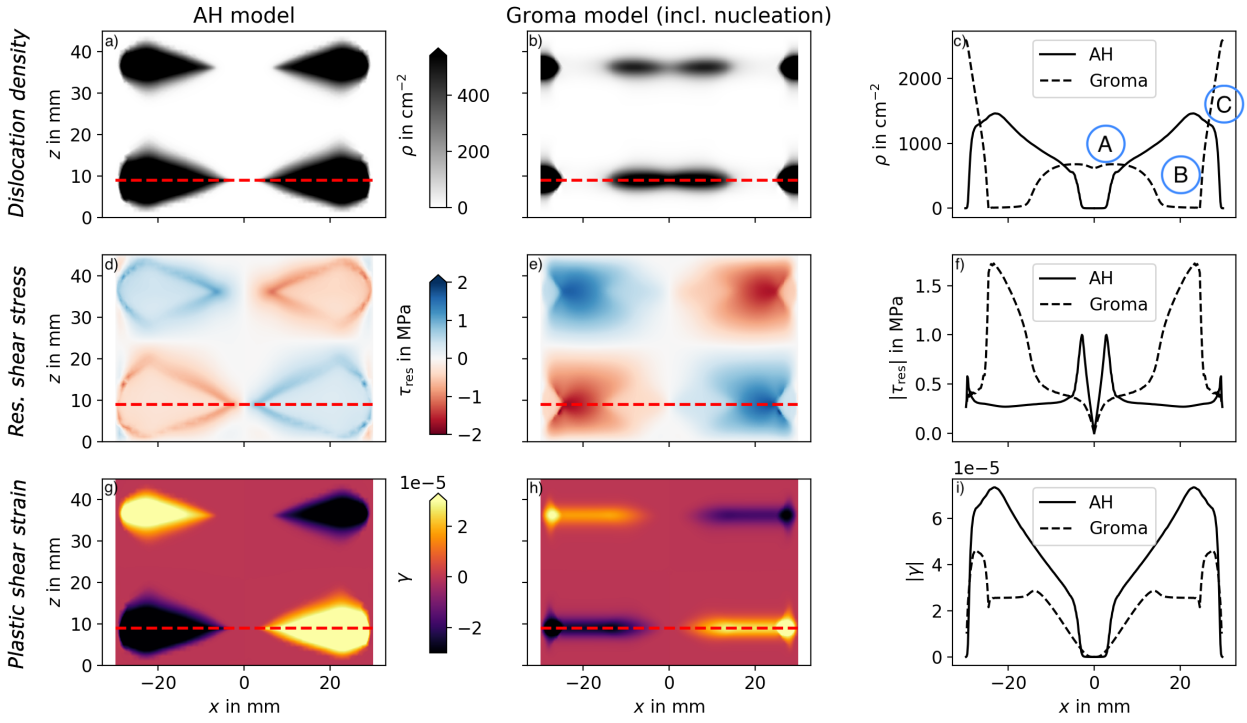

Figure 1.4: Comparison between AH model and Groma model including a source term: the top row shows the density, the middle row the resolved shear stress and the bottom row depicts the plastic strain. The left column are results for both models plotted along the red, dashed lines.

also obvious in the results of the resolved shear stress. Fig. 1.4d and Fig. 1.4e shows the resolved shear stress τ_{res} field for the basal slip system with respect to the dislocation density distribution in Fig. 1.4a and Fig. 1.4b. In the AH model, ρ_{m} will initially increase at the four stress hot spot (see Fig. 1.2b) and then decrease as a consequence of plastic relaxation

which can be observed in the shape change (compared Fig. 1.2b and Fig. 1.4d); it reaches the state shown in Fig. 1.4d. As a result of this "stress transfer", a substantial increase in dislocation density by nucleation of new dislocations takes place in regions where originally the initial stress was low. As opposed to that, in the Groma model, dislocation accumulations occur close to the surface and close to the crystal axis. The reason for this behavior is that dislocations are nucleated where the stress is highest, but then move away, driven by shear stresses. They accumulated where the shear stress is low (see Fig. 1.4e and Fig. 1.4f) and form quasi-stationary pile-up structures. It ultimately leads to a depleted zone where in the AH model the density is highest (see label B in Fig. 1.4c).

Is this consistent with the results for the plastic shear? For the AH model, plastic strain co-evolves with the nucleation of dislocation density and therefore, as expected, has roughly the same shape as the dislocation density (see Fig. 1.4g and Fig. 1.4i). The Groma model behaves quite differently as the AH model. In the Groma model, the plastic strain is caused by dislocation *motion* and is high in the regions which were swept by dislocation (see Fig. 1.4h and Fig. 1.4i). These are, for this example, exactly the regions where no dislocations are present any more. This is the expected behavior which is consistent with basic dislocation dynamics. Thus, the comparison of the two different simulations revealed that the flow of dislocation in the crystal during growth can not be neglected, as it is done in the AH model. The dislocation motions controls the distribution of dislocation inside the crystal and makes it possible that dislocations can move even to places where originally the stress was low, such as the surfaces or the central region. However, the Groma model has some limitation, as already above stated: e.g., the source term is just an approximation which cannot capture the whole mechanisms of dislocation nucleation; furthermore, dislocations are only assumes to be straight lines. And last but not least, the simulation only considers basal plane dislocation while there are many more types of dislocations in reality that also need to be taken into account.

1.5 Example 2: Dislocation flow between veins

1.5.1 A brief introduction to dislocation patterning and the similitude principle

Under certain conditions it is observed that dislocations tend to form heterogeneous but regular structures, some of which are termed "dislocations patterns". They are observed both in metals as well as in semiconductors. The micrographs in Fig. 1.5 show examples of such structures. These dislocation patterns can occur, e.g., as approximately periodic dislocation agglomerations or sharply distinguishable cell (e.g., Fig. 1.5c) or "labyrinth" structures (Fig. 1.5h). The common feature is that all of these structures are characterized by clusters of very high dislocation density alternating with regions of very low (or zero) density. These dislocation formations are usually 'metastable' structures which mostly persist upon unloading. One of the remarkable features is that the cell sizes Λ – regardless material, loading condition or temperature – are always related to the applied stress τ_{ext} through the 'law of similitude' [52, 53] by $\Lambda = DaGb/\tau_{\text{ext}}$, where usually the constant $D = 10 \dots 20$ and G is the shear modulus, and $a \approx 0.3$ is the non-dimensional coefficient relating flow stress and

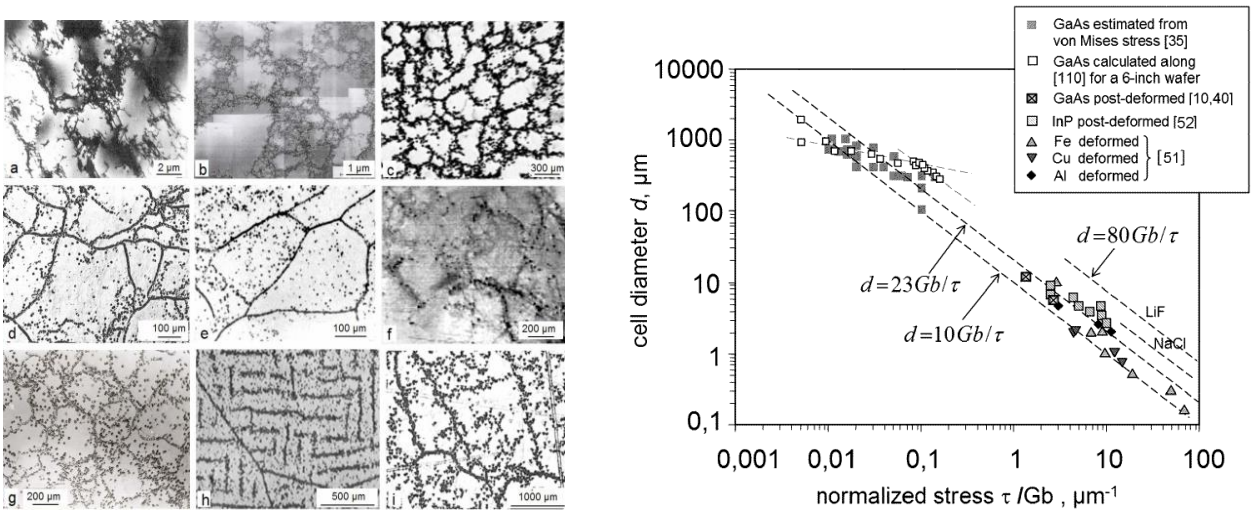

Figure 1.5: Dislocation organize themselves into patterns as e.g. cell structure, independent of the material or loading condition(left). The cell size is related to the applied stress through the 'similitude relation' (right). Images taken with permission from Rudolph [4].

dislocation density ρ in the Taylor relationship $\tau = aGb\sqrt{\rho}$. This has been known for plastically deformed metals for about half a century [54] but is also observed in semiconductors as pointed out more recently by Rudolph [4, 5]: e.g. in GaAs dislocations arrange themselves in experimentally observable cellular structures of diameter in between $100 \ldots 1000\,\mu\text{m}$. Although the regular (sometimes fractal) appearance is visually interesting, these dislocation structures deteriorate the electronic and mechanical properties of semiconductors, and their formation needs to be prevented as far as possible. Hence, understanding the mechanisms leading to the occurrence of patterns is crucial for being able to prevent such structures. Rudolph [4] suggested to relate the origin of this phenomenon to the same mechanisms as in the case of metals (where cells form roughly in the $1\,\mu\text{m}$ to $10\,\mu\text{m}$ size range, see Fig. 1.5 (left)). The different cell size regimes, i.e. mm-range for semiconductors and μm-range for metals, is related to the very different dislocation densities at saturation which result in different stresses due to the Taylor relationship (Fig. 1.5 (right)). In the case of SiC dislocation cell structures have also been reported in the past for materials exhibiting dislocation densities in the mid $10^4\,\text{cm}^{-2}$ to low $10^5\,\text{cm}^{-2}$ range, however, basically no attention has been paid to describe the dislocation microstructure in terms of such networks or cells. At lower dislocation densities in the mid $1 \times 10^3\,\text{cm}^{-2}$ range as it is typical for best commercial SiC wafer materials, the cell structure is difficult to visualize and mainly occurs in defective areas where dislocation bundles occur. So far, no detailed theoretical concept or computational model of dislocation cell formation in semiconductor materials exists. There is, however, a great need to explain and therefore to be able to take countermeasures against the formation of dislocation entanglements, which also has been recognized in the literature: for instance, the 2014 edition of the book *Extended Defects in Semiconductors* by Holt and Yacobi [55] strongly emphasizes within the last sentence of the section *Major Persisting Issues* "... The need for a theoretical framework for this phenomenon [cellular dislocation structures] ...". Encouraged by this general viewpoint, we take it as an worthwhile task to transfer modeling

of dislocation patterning from metals to the semiconductor case.

1.5.2 Physical system and model setup

Approaches that are able to predict dislocations patterning are – even in the modeling community for dislocation mediated metal plasticity simulation – very scarce: even discrete simulation methods are due to the computational cost generally not able to predict the evolution of dislocation patterns. This is why in the following a CDD model will be used to demonstrate some of the most important mechanisms involved during formation of dislocation patterns. The first stage, i.e., the formation of such stable dislocation agglomerations has already been investigated in [34] and for a different formulation also in [56] where it was shown that the above CDD model is indeed able to simulate this.

As a model system we now assume that already a stable wall-like structure (e.g., a cell wall or the wall of a persistent slip band) exists. A dislocation dynamics model must then be able to represent the motion of dislocations between these constraining walls, similar to the situation investigated in [38]. The experimental results from Mughrabi [57] shown in Fig. 1.6a, illustrate the walls structure in a so-called persistent slip band (PSB) which consist of dipolar edge dislocation configurations. The dislocations gliding in the channels between the walls have mainly screw orientation. In cell structures, the cell walls may have a different dislocation content, however, the ability to represent bowing out of dislocations and glide in between the walls is equally important. In what follows we will now demonstrate that the CDD model is able to represent the bowing-out/gliding mechanism, which is a prerequisite for predicting the formation for cell or wall structures.

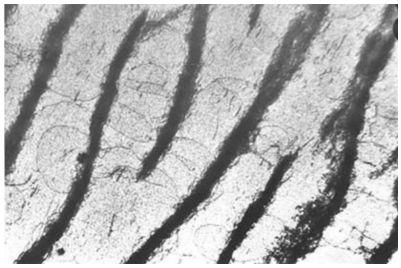

(a)

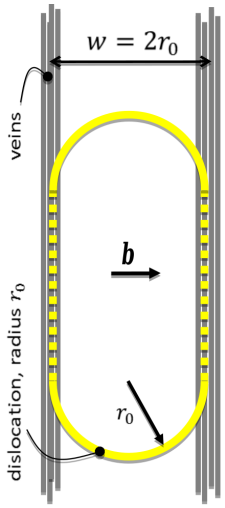

(b)

Figure 1.6: a) TEM micrograph showing walls of PSBs (dark) [57] and gliding of screw segments between walls; b) Schematic of dislocation vein structure made up of extended edge dipoles and glide screw dislocation of radius r_0. The channel width is $w = L_x$.

1.5.3 Geometry and initial values

The geometry is chosen to be rectangular with the channel width L_x and the channel length L_y (see Table 1.1 for all numerical values and used material parameters). The system is

Table 1.1: Parameters for dislocation flow between veins.

Parameter	Value
System size L_x	$1 \times 10^{-5}\,\mathrm{m}$
System height L_y	$2 \times 10^{-5}\,\mathrm{m}$
Loops radius r_0	$2 \times 10^{-6}\,\mathrm{m}$
Standard deviation s	$7 \times 10^{-6}\,\mathrm{m}$
Burgers vector modulus b	$0.256 \times 10^{-9}\,\mathrm{m}$
Drag coefficient B	$5 \times 10^{-8}\,\mathrm{Pa \cdot s}$
Shear modulus G	$128 \times 10^{9}\,\mathrm{Pa}$

periodic in y direction, i.e., dislocations exiting the system at the top will flow back in at the bottom. In horizontal direction the boundaries are impenetrable for dislocations, which is modeled by a horizontal velocity profile that is zero directly at the boundaries, constant inside the channel with a value of v_0, and has a smooth transition in between:

$$v = v_0 \left(\frac{2}{1 + e^{-(x+L_\mathrm{x}/2)\beta}} - 1 \right) \left(\frac{2}{1 + e^{-(L_\mathrm{x}/2-x)\beta}} - 1 \right), \tag{1.19}$$

with $v_0 = 0.4\,\mathrm{m\,s^{-1}}$, $\beta = 0.004$. Within the present work we ignore all dislocation interactions and concentrate exclusively on the 'kinematics', that is, how curved and connected lines move and evolve in space and time without interactions.

In order to consistently representing a system of curved and connected lines in a coarse-grained continuum manner, we obtain dislocation density distributions (such as ρ_t) by first defining a distribution of a number of mathematical dislocation loops. This is followed by convolution along the loops' lines with a Gaussian normal distribution function $\left(s\sqrt{2\pi}\right)^{-1} \exp\left(-\xi^2/2s^2\right)$, where s is the width of the distribution and ξ is the distance perpendicular to the loop. This effectively "smears out" the line prependicular to it. By multiplication of the dislocation density with the normalized radial unit vector or division by its radius, r, we can determine the dislocation density vector $\boldsymbol{\varrho}$ or the curvature density $q_t = \rho_t/r$, respectively. CDD initial values are obtained by summing up the individual fields. Initial values with two dislocation loops and 50 dislocation loops for our simulation are shown in Fig. 1.7 and Fig. 1.8. The curvature, i. e., 1/radius of a line is obtained in a postprocessing step from $k = q/\rho$; it is not defined in regions where the density is zero (compare the right most plot in Fig. 1.7). More details on the process of creating consistent initial values can be found in [33, 34].

1.5.4 Results and discussion

Because of the zero velocity in the walls and the smooth transition from $v = 0$ to a constant velocity v_0 further away from the wall, the velocity field acts such that dislocations are

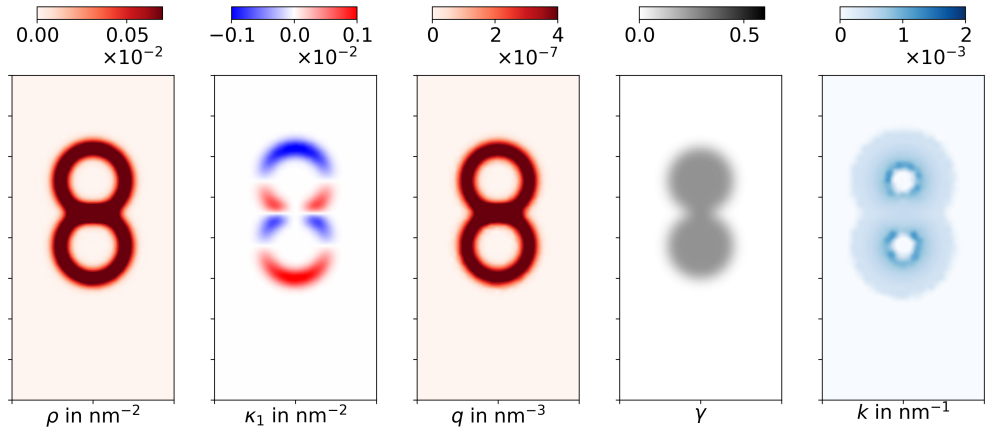

Figure 1.7: Initial CDD field values for two quasi-discrete dislocation loops. From left to right: total density, edge GND density component, curvature density, plastic slip, curvature.

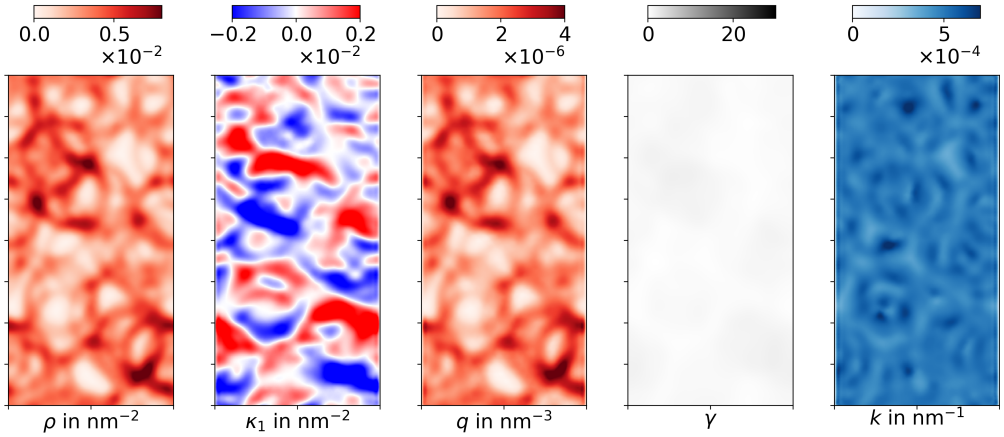

Figure 1.8: Initial CDD field values for a distribution of 50 dislocation loops. From left to right: total density, edge GND density component, curvature density, plastic slip, curvature.

first slowed down on their way towards the walls and eventually freeze in their motion so that they cannot enter the walls. Fig. 1.9 and Fig. 1.10 present the relations among the four CDD variables during dislocation evolution. The two-loop system is not fundamentally different from the 50-loop system but makes it easier to understand the meaning of the different fields. Initially, one can observe free loop expansion inside the domain because of the constant velocity. Since we neglect interaction between dislocations and assume that they or on different but near-by slip planes in their respective averaging volumes, they will pass through each other during expansion. Later, at time $t = 0.01$, we can observe that dislocation will reach the left and right boundaries and begin to a pile-up at these walls while they still expand in the vertical direction (see figure 1.9 and figure 1.10). An interesting feature is the formation of pile-ups of bent lines at walls: when expanding dislocation loops touch the left and right boundaries, they bend and adjust to the shape of the walls. Because of that, the values of curvature density q at these areas are larger than inside area. Line pile-ups of dislocation density can be seen in the left and right boundaries and even clearer as a banded

structure at time $t = 0.025$. The dislocation density ρ has a high value in the vicinity of the walls because of the density from piled-up dislocations. The threading edge segments, i.e., density with approximately horizontal orientation, are segments from expanding loops. Therefore, they become more straight, which also shows in their reduced curvature (last column of Fig. 1.9 and Fig. 1.10). Investigating the curvature $k = q/\rho$, because of the impenetrable walls we observe that the screw segments are straight with the curvature value $k = 0$ at walls and we find a non-zero curvature shortly before the surface where dislocations need to bend strongly.

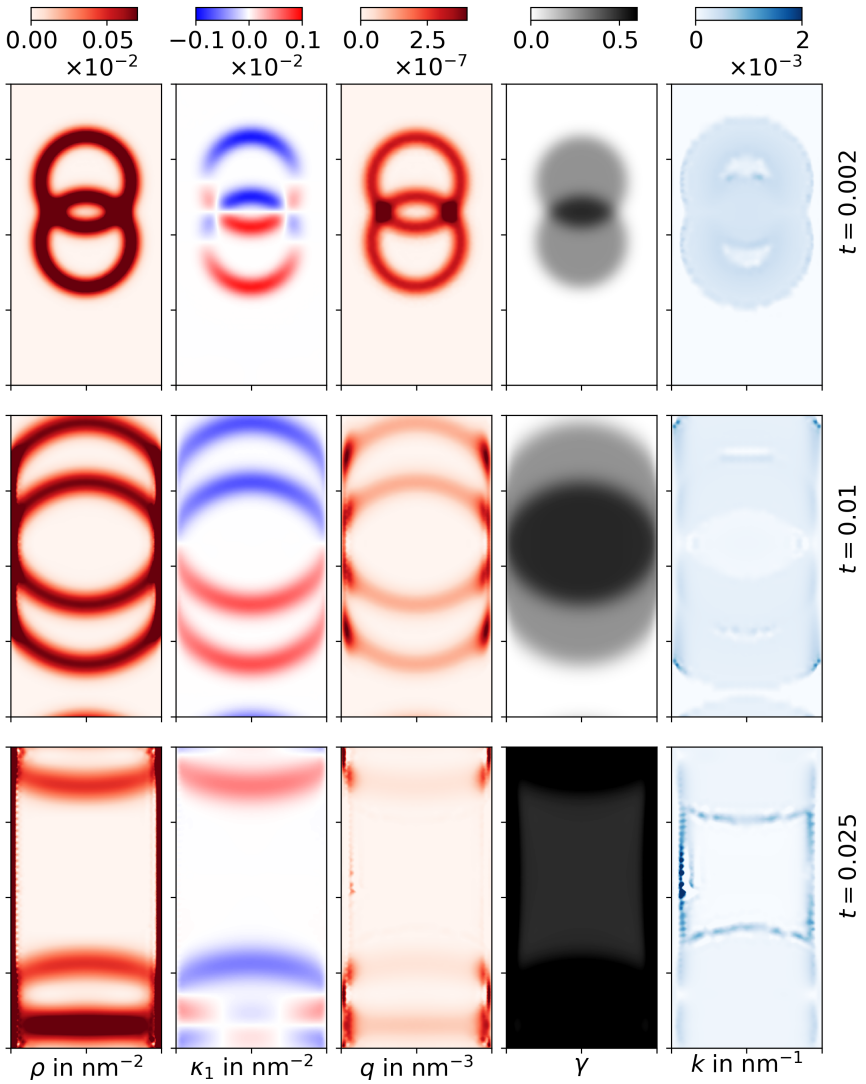

Figure 1.9: Two mobile dislocation loops expansion in the channel.

The plastic slip γ – which is the pendant of the plastic strain on the level of the individual slip plane – shows clearly that it is proportional to the slipped area. Where two loops overlap, the value of γ is doubled. The system with 50 loops, on the other hand, shows nearly homogeneous plasticity in the inside of the channel and a larger accumulation of plastic slip directly at the boundaries. This is due to the fact that the high curvature density scales is

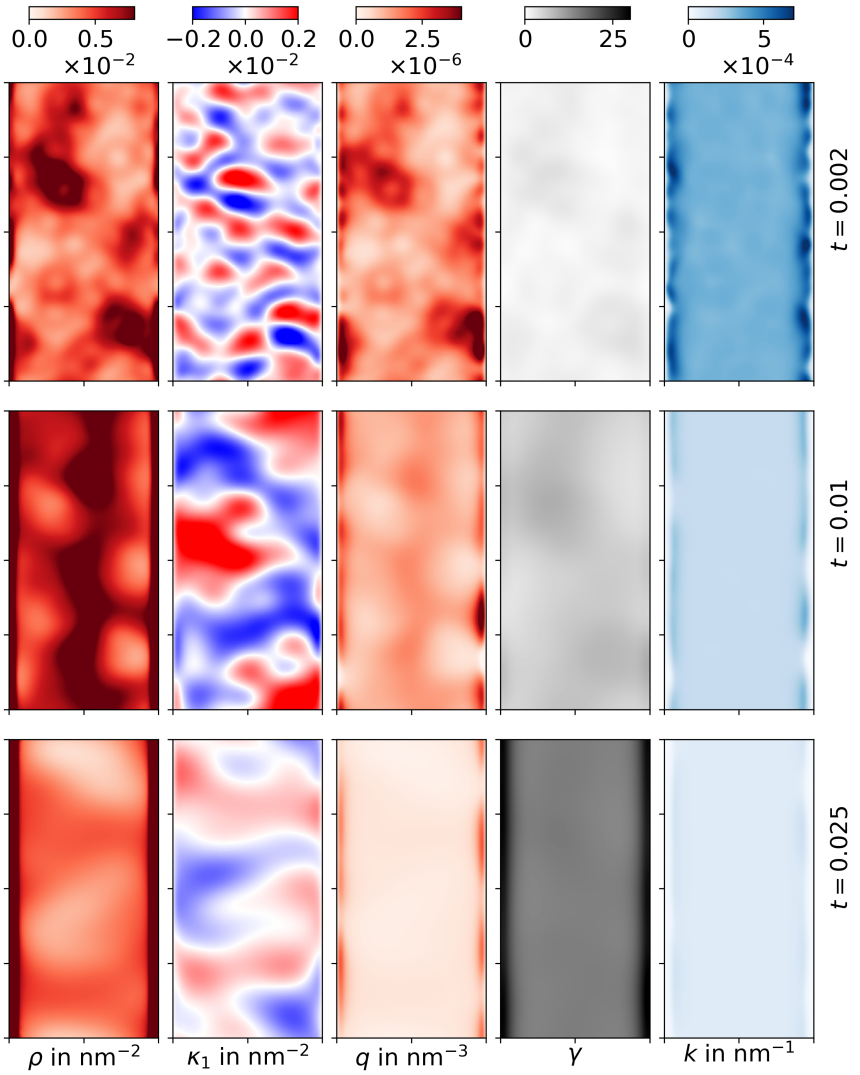

Figure 1.10: Fifty mobile dislocation loops expansion in the channel.

responsible for additional line length production.

How do these microscopic field variables relate to average quantities on the macroscopic system scale? Fig. 1.11 shows the total dislocation line length $l = \int_A \rho \, \mathrm{d}A$ versus time. To validate our model results we construct two extreme cases:

(i) There is only free loops expansion as if no boundaries and interactions are present. This results in a linear line length increase $L = N_\mathrm{d} 2\pi \, (r_0 + vt)$ (with N_d the number of loops and v the velocity) and is shown as the tangent on the left of the plot in Fig. 1.11.

(ii) Loops have a very large radius such that the threading edge segments can be considered as straight. Then these segements move and at the same time deposit straight screw segments at the boundaries, as if it were a rectangular loop. This yields a line length of $L = N_\mathrm{d} \, (\pi w + 4vt + 2w)$ with w the width of the channel. This is shown as the tangent on the right of the plot in Fig. 1.11.

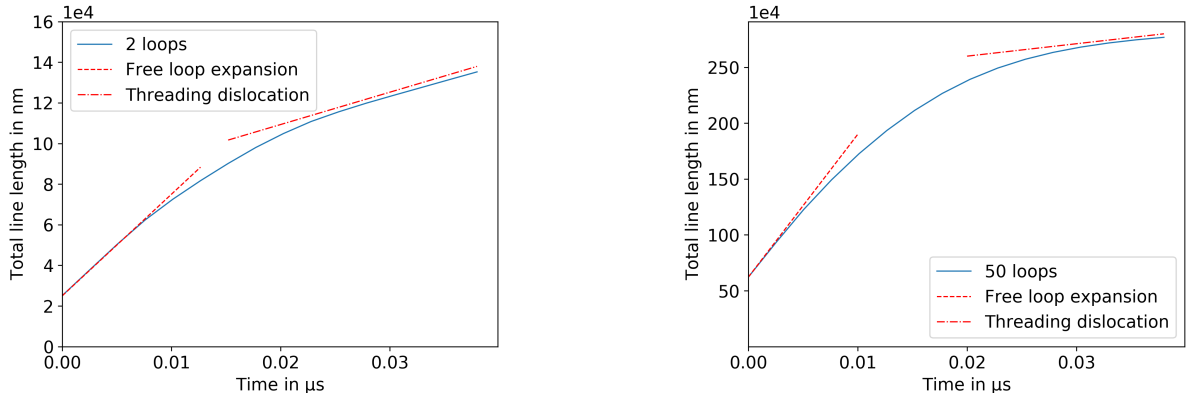

Figure 1.11: Total line length vs time. The two tangents denote the line length assuming (i) only free loop exapansion without any boundaries and (ii) only straight edge segments that are connected by straight screw segments as in a rectangular loop.

One can observe that the simulation reproduces the correct rate of line length at the beginning of the simulation and towards the end; in between is a larger transition region. This clearly demonstrates that the complex interplay between dislocation loop expansion, dislocation motion, line bending and deposition at a boundary can all be predicted by this CDD model. Additionally, without dislocation interactions, the system is just a superposition of individual loops, even in cases where the individual loops can no longer be distinguished. Using just the Groma model could not work because the line length production due to the threading edge dislocations can not be represented and the total line length in the system would stay constant. How would the AH model have performed? A direct comparison is difficult because the CDD model can operate even without stresses and just by prescribing a velocity. Assuming a constant shear stress, the AH model would not be able to represent the deposition of density at the boundary, similar to what was shown in Fig. 1.4. Furthermore, it would not be possible to interpret the resulting density or plastic strain configuration in terms of geometrical properties of dislocations lines. Since dislocations are the carrier of plastic deformation, we see the lag of interpretability as one of the big drawbacks of any purely phenomenological continuum model – irrespective of the quality of the overall predictions.

1.6 Summary and Conclusion

An overview over current state of the art modeling techniques for predicting defects in semiconductors has been presented. Putting a focus on systems of dislocations, it was discussed that it might be very lucrative to apply simulations methods from the metal plasticity domain to the domain of semiconductors. In this context, a number of state of the art methods for predicting the dislocation dynamics in a continuum frame work were introduced and critically discussed. In particular the comparison with one of the most established simulation model used in the semiconductor domain, the Alexander-Haasen model, demonstrated that it is very important to be aware of the limitations and the range of applicability of a model: the Alexander-Haasen model is not able to predict fluxes of dislocations, which in many

applications might be a strong limitation.

Discussing modeling approaches in the context of dislocation pattern formation, we demonstrated that the introduced CDD model is able to represent many important dislocation features that also can be clearly interpreted in terms of geometrical features of curved lines. Nonetheless, the current CDD theory still has not been applied to general system in three dimensions. This will require detailed work on extracting data from DDD and MD simulations that can then be used as input for dislocation interaction formulations. Nonetheless, a continuum model which operates on length and time scales comparable to experimental ones also might be very well able to act as a link between theory, modeling and experiment. In particular experimental data is, of course, the ultimate benchmark for any model. Therefore one might by tempted to say that a good simulation model need not exactly reproduce experimental results; rather, a good simulation model is a model that can be easily interpreted as well as parameterized and directly validated by experiments, both on the microscopic and macroscopic scale.

Bibliography

[1] William C Dash. Growth of silicon crystals free from dislocations. *Journal of Applied Physics*, 30(4):459–474, 1959.

[2] K Hashio, S Sawada, M Tatsumi, K Fujita, and S Akai. Low dislocation density si-doped gaas single crystal grown by the vapor-pressure-controlled czochralski method. *Journal of crystal growth*, 173(1-2):33–41, 1997.

[3] Peter Rudolph. *Handbook of crystal growth: Bulk crystal growth*. Elsevier, 2014.

[4] P Rudolph. Dislocation cell structures in melt-grown semiconductor compound crystals. *Crystal Research and Technology: Journal of Experimental and Industrial Crystallography*, 40(1-2):7–20, 2005.

[5] Peter Rudolph. Dislocation patterning and bunching in crystals and epitaxial layers-a review. *Crystal Research and Technology*, 52(1):1600171, 2017.

[6] Govindhan Dhanaraj, Kullaiah Byrappa, Vishwanath Prasad, and Michael Dudley. *Springer handbook of crystal growth*. Springer Science & Business Media, 2010.

[7] J Łażewski, PT Jochym, P Piekarz, M Sternik, K Parlinski, J Cholewiński, P Dłużewski, and S Krukowski. Dft modelling of the edge dislocation in 4h-sic. *Journal of Materials Science*, 54(15):10737–10745, 2019.

[8] SI Rao, C Varvenne, C Woodward, TA Parthasarathy, D Miracle, ON Senkov, and WA Curtin. Atomistic simulations of dislocations in a model bcc multicomponent concentrated solid solution alloy. *Acta Materialia*, 125:311–320, 2017.

[9] E Oren, E Yahel, and G Makov. Dislocation kinematics: a molecular dynamics study in cu. *Mod. Simul. Mater. Sci. Eng*, 25:025002, 2017.

[10] Xiaowang Zhou, Donald K Ward, Bryan M Wong, F Patrick Doty, and Jonathan A Zimmerman. Molecular dynamics studies of dislocations in cdte crystals from a new bond order potential. *The Journal of Physical Chemistry C*, 116(33):17563–17571, 2012.

[11] Chen Chen, Haitao Li, Henggao Xiang, and Xianghe Peng. Molecular dynamics simulation on b3-gan thin films under nanoindentation. *Nanomaterials*, 8(10):856, 2018.

[12] H. D. Espinosa, M. Panico, S. Berbenni, and K. W. Schwarz. Discrete dislocation dynamics simulations to interpret plasticity size and surface effects in freestanding fcc thin films. *International Journal of Plasticity*, 22(11):2091–2117, 2006.

[13] V. V. Bulatov, W. Cai, J. Fier, and M. Hiratani. Scalable line dynamics in ParaDiS. *Proceedings of the 2004 ACM/IEEE conference on Supercomputing*, 2004.

[14] D. Weygand, L. H. Friedman, E. Van der Giessen, and A. Needleman. Aspects of boundary-value problem solutions with three-dimensional dislocation dynamics. *Modelling Simul. Mater. Sci. Eng.*, 10(4):437–468, 2002.

[15] B Devincre and M Condat. Model validation of a 3D simulation of dislocation dynamics: Discretization and line tension effects. *Acta Metall Mater*, 40(10):2629–2637, October 1992.

[16] C. Motz, D. Weygand, J. Senger, and P. Gumbsch. Initial dislocation structures in 3-d discrete dislocation dynamics and their influence on microscale plasticity. *Acta Materialia*, 57(6):1744–1754, 2009.

[17] D. Mordehai, E. Clouet, M. Fivel, and M. Verdier. Introducing dislocation climb by bulk diffusion in discrete dislocation dynamics. *Philosophical Magazine*, 88(6):899–925, 2008.

[18] Wai Yuen Fu, Colin J Humphreys, and Michelle A Moram. Panic: a 3d dislocation dynamics model for climb and glide in epitaxial films and heterostructures. *arXiv preprint arXiv:1406.0780*, 2014.

[19] G. Boussinot, Y. L. Bouar, and A. Finel. Phase-field simulations with inhomogeneous elasticity: Comparison with an atomic-scale method and application to superalloys. *Acta Mater.*, 58:4170 – 4181, 2010.

[20] A. Hunter, F. Saied, C. Le, and M. Koslowski. Large-scale 3d phase field dislocation dynamics simulations on high-performance architectures. *Int. J. H.P.C. Appl.*, 25:223–235, 2011.

[21] H Alexander and P Haasen. Dislocations and plastic flow in the diamond structure. In *Solid state physics*, volume 22, pages 27–158. Elsevier, 1969.

[22] I. Yonenaga and K. Sumino. Dislocation dynamics in the plastic deformation of silicon crystals i. experiments. *Physica status solidi (a)*, 50(2):685–693, 1978.

[23] M. Suezawa, K. Sumino, and I. Yonenaga. Dislocation dynamics in the plastic deformation of silicon crystals. ii. theoretical analysis of experimental results. *physica status solidi (a)*, 51(1):217–226, 1979.

[24] T. Ide, H. Harada, Y. Miyamura, M. Imai, S. Nakano, and K. Kakimoto. Relationship between dislocation density and oxygen concentration in silicon crystals during directional solidification. *Crystals*, 8(6):244, 2018.

[25] N Miyazaki and S Okuyama. Development of finite element computer program for dislocation density analysis of bulk semiconductor single crystals during czochralski growth. *Journal of crystal growth*, 183(1-2):81–88, 1998.

[26] B Gao, S Nakano, and Koichi Kakimoto. Highly efficient and stable implementation of the alexander–haasen model for numerical analysis of dislocation in crystal growth. *Journal of Crystal Growth*, 369:32–37, 2013.

[27] Bing Gao and Koichi Kakimoto. Dislocation-density-based modeling of the plastic behavior of 4h–sic single crystals using the alexander–haasen model. *Journal of Crystal Growth*, 386:215–219, 2014.

[28] I Groma, FF Csikor, and M Zaiser. Spatial correlations and higher-order gradient terms in a continuum description of dislocation dynamics. *Acta Materialia*, 51(5):1271–1281, 2003.

[29] Thomas Hochrainer, Stefan Sandfeld, Michael Zaiser, and Peter Gumbsch. Continuum dislocation dynamics: towards a physical theory of crystal plasticity. *Journal of the Mechanics and Physics of Solids*, 63:167–178, 2014.

[30] S. Sandfeld, T. Hochrainer, P. Gumbsch, and M. Zaiser. Numerical implementation of a 3d continuum theory of dislocation dynamics and application to micro-bending. *Philosophical Magazine*, 90(27-28):3697–3728, 2010.

[31] Stefan Sandfeld, Thomas Hochrainer, Michael Zaiser, and Peter Gumbsch. Continuum modeling of dislocation plasticity: Theory, numerical implementation, and validation by discrete dislocation simulations. *Journal of materials research*, 26(5):623–632, 2011.

[32] Stefan Sandfeld, Mehran Monavari, and Michael Zaiser. From systems of discrete dislocations to a continuous field description: stresses and averaging aspects. *Modelling and Simulation in Materials Science and Engineering*, 21(8):085006, 2013.

[33] Stefan Sandfeld and Giacomo Po. Microstructural comparison of the kinematics of discrete and continuum dislocations models. *Modelling and Simulation in Materials Science and Engineering*, 23(8):085003, 2015.

[34] Stefan Sandfeld and Michael Zaiser. Pattern formation in a minimal model of continuum dislocation plasticity. *Modelling and Simulation in Materials Science and Engineering*, 23(6):065005, 2015. URL `http://stacks.iop.org/0965-0393/23/i=6/a=065005`.

[35] Michael Zaiser. Local density approximation for the energy functional of three-dimensional dislocation systems. *Physical Review B*, 92(17):174120, 2015.

[36] Mehran Monavari, Michael Zaiser, and Stefan Sandfeld. Comparison of closure approximations for continuous dislocation dynamics. *MRS Online Proceedings Library Archive*, 1651, 2014.

[37] G. I. Taylor. The mechanism of plastic deformation of crystals. part i.—theoretical. *Proceedings of the Royal Society of London. Series A, Containing Papers of a Mathematical and Physical Character*, 145(855):362–387, 1934.

[38] Mehran Monavari, Stefan Sandfeld, and Michael Zaiser. Continuum representation of systems of dislocation lines: a general method for deriving closed-form evolution equations. *J. Mech. Phys. Solids*, 95:575 – 601, 2016. ISSN 0022-5096. doi: http://dx.doi.org/10.1016/j.jmps.2016.05.009. URL `http://www.sciencedirect.com/science/article/pii/S0022509615301903`.

[39] Binh Duong Nguyen, Alexander M Rausch, Johannes Steiner, Peter Wellmann, and Stefan Sandfeld. On the importance of dislocation flow in continuum plasticity models for semiconductor materials. *Journal of Crystal Growth*, page 125414, 2019.

[40] Radan Sedláček, Jan Kratochvíl, and Ewald Werner. The importance of being curved: bowing dislocations in a continuum description. *Philosophical Magazine*, 83(31-34): 3735–3752, 2003.

[41] Anter El-Azab. Statistical mechanics treatment of the evolution of dislocation distributions in single crystals. *Physical Review B*, 61(18):11956, 2000.

[42] Amit Acharya and Anish Roy. Size effects and idealized dislocation microstructure at small scales: predictions of a phenomenological model of mesoscopic field dislocation mechanics: Part i. *Journal of the Mechanics and Physics of Solids*, 54(8):1687–1710, 2006.

[43] E Kröner. Benefits and shortcomings of the continuous theory of dislocations. *International journal of solids and structures*, 38(6-7):1115–1134, 2001.

[44] E. van der Giessen and A. Needleman. Discrete dislocation plasticity: a simple planar model. 3(5):689–735. doi: 10.1088/0965-0393/3/5/008.

[45] I Groma. Link between the microscopic and mesoscopic length-scale description of the collective behavior of dislocations. *Physical Review B*, 56(10):5807, 1997.

[46] Ekkehart Kröner. *Kontinuumstheorie der versetzungen und eigenspannungen*, volume 5. Springer, 1958.

[47] Stefan Sandfeld and Giacomo Po. Microstructural comparison of the kinematics of discrete and continuum dislocations models. 23(8):085003. doi: 10.1088/0965-0393/23/8/085003.

[48] Anter El-Azab, Jie Deng, and Meijie Tang. Statistical characterization of dislocation ensembles. *Philosophical Magazine*, 87(8-9):1201–1223, 2007.

[49] Ekkehart Kröner. Der fundamentale zusammenhang zwischen versetzungsdichte und spannungsfunktionen. *Zeitschrift für Physik*, 142(4):463–475, 1955.

[50] Zibing Zhang, Jing Lu, Qisheng Chen, and V Prasad. Thermoelastic stresses in sic single crystals grown by the physical vapor transport method. *Acta Mechanica Sinica*, 22(1):40–45, 2006.

[51] Z. Li and R. C. Bradt. The single crystal elastic constants of hexagonal SiC to 1000°C. *International Journal of High Technology Ceramics*, 4(1):1 – 10, 1988.

[52] M Sauzay and Ladislas P Kubin. Scaling laws for dislocation microstructures in monotonic and cyclic deformation of fcc metals. *Progress in Materials Science*, 56(6):725–784, 2011.

[53] M. Zaiser and S. Sandfeld. Scaling properties of dislocation simulations in the similitude regime. *Modelling and Simulation in Materials Science and Engineering*, 22(6), 2014. ISSN 09650393. doi: 10.1088/0965-0393/22/6/065012. URL `http://iopscience.iop.org/0965-0393/22/6/065012/`.

[54] H Mughrabi. Dislocation wall and cell structures and long-range internal stresses in deformed metal crystals. *Acta metallurgica*, 31(9):1367–1379, 1983.

[55] David B Holt and Ben G Yacobi. *Extended defects in semiconductors: electronic properties, device effects and structures*. Cambridge University Press, 2007.

[56] Shengxu Xia and Anter El-Azab. Computational modelling of mesoscale dislocation patterning and plastic deformation of single crystals. 23(5):055009. doi: 10.1088/0965-0393/23/5/055009.

[57] Hael Mughrabi. Cyclic slip irreversibilities and the evolution of fatigue damage. *Metallurgical and Materials Transactions B*, 40(4):431–453, 2009.